Supporting Information

A Cyclic Ion Mobility – Mass Spectrometry System

Kevin Giles, Jakub Ujma, Jason Wildgoose, Steven Pringle, Keith Richardson, David Langridge and Martin Green

Waters Corporation, Stamford Avenue, Altrincham Road, Wilmslow SK9 4AX UK

Table of Contents

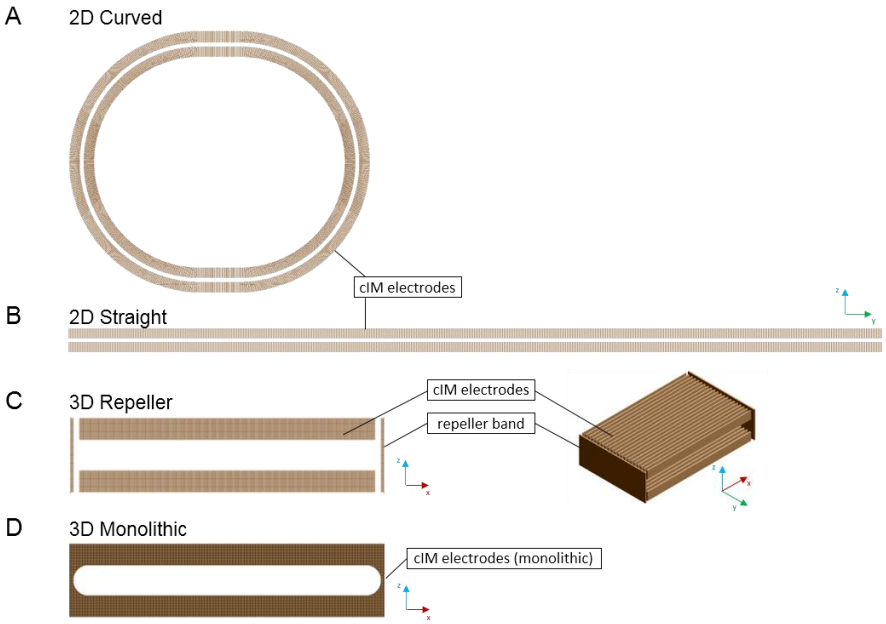

Figure S1. SIMION (v8.1, Scientific Instrument Services, Inc., Ringoes, NJ USA) geometries used to evaluate cIM operation. Models A and B were generated to compare the IM separation along a closed-loop, "curved" path (A) and a "straight" path (B) of the same length. Both models feature 2D planar symmetry along the x-axis. The width of the separator (x-dimension) is essentially infinite therefore the ions experience no edge effects. The 3D models were prepared to evaluate different rectangular electrode designs (C, D) and in particular the effect of ion confinement in the x-direction. The zx-planes shown in C and D correspond to a cross-section of the 3D model with a linear y-dimension separation path of 98 cm.

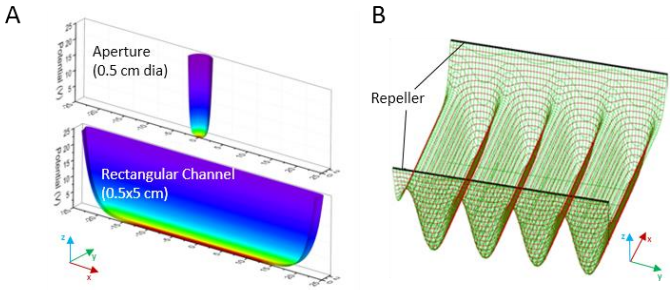

Figure S2. A: simulation of ion confinement potential in a SRIG TWIM device (top) and in the cIM rectangular channel geometry (bottom). The ~10x increase in capacity of the rectangular channel equates to around 2 million singly charged ions. B: SIMION simulation showing the shape of the TW potential and DC confinement in the x-direction.

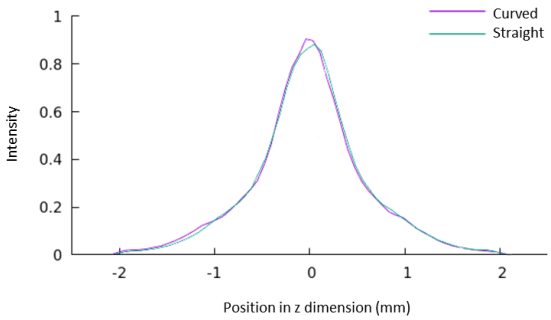

Figure S3. Simulated spatial distributions of two singly charged ions (491 m/z, CCS values of 205.3 and 208.5 $Å^2$) in the z-dimension of the "curved" and "straight" geometry. Trajectories of 28 ions were simulated to generate these data. The distributions shown correspond to the histogram of an ion's position in the z-dimension recorded every 0.37 µs during a 5 ms drift along each geometry. Both simulations used TW heights of 35V and TW velocities of 375 m/s at 1.8 mbar of N_2. z=0 mm corresponds to the equidistant position between the inner and outer cIM electrodes in the "curved" geometry, and the top and bottom electrodes in the "straight" geometry.

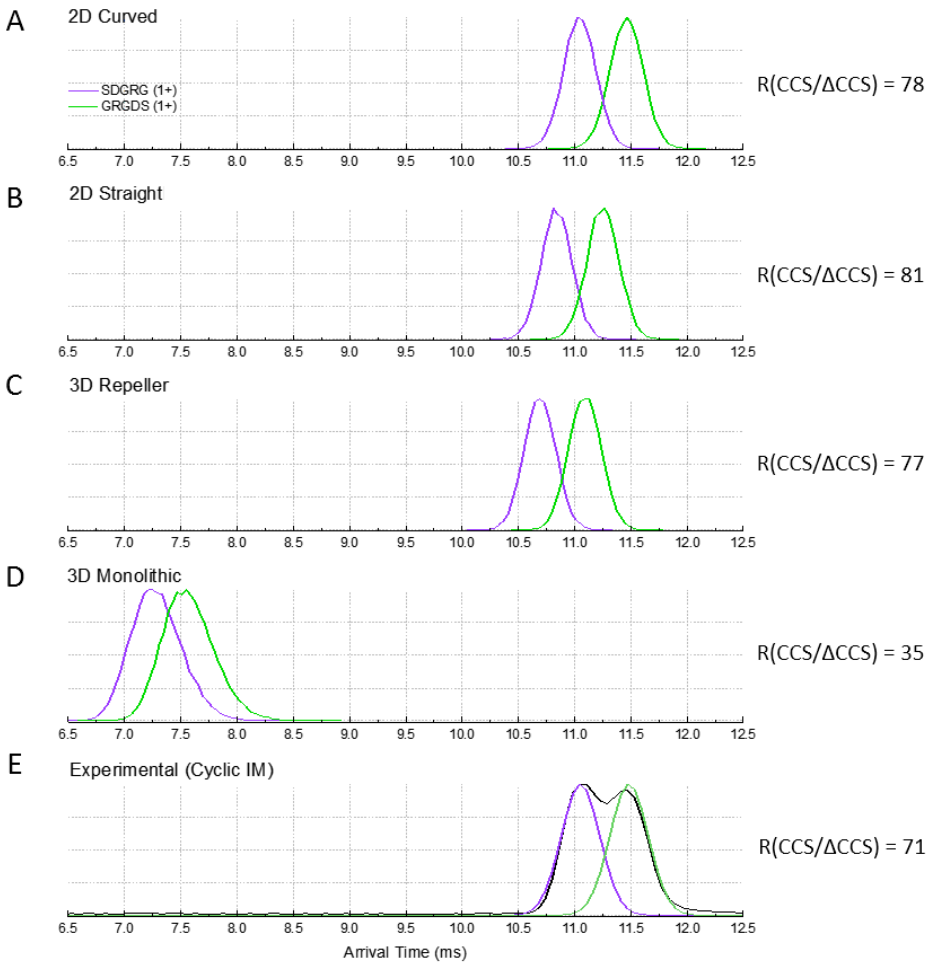

Figure S4. SIMION simulated (A-E) and experimental (F) arrival time distributions (ATDs) of the inverse sequence singly charged peptides (SDGRG and GRGDS) with CCS values of 205.3 and 208.5 $Å^2$. The corresponding geometry models are presented in the Figure S1. Simulations A and B show the ion separation after 98 cm drift along the "curved" and "straight" geometry. There essentially no difference in resolution performance, as indicated by the R(CCS/ΔCCS) values. This result implies that different adjacent plate spacing between inner and outer electrodes, as well as different radial trajectories of ions do not substantially reduce the performance of the cIM over an equivalent linear TWIM device. Simulations C and D highlight the importance of using a DC electrode for confinement in the x-direction, rather than a monolithic, closed, electrode geometry. In these simulations, a weak electric field (0.1 V/mm) was applied in the x-direction to push ions towards the edge of the device, approximating the effect of space charge. Clearly, the monolithic electrode (D) design would be expected to cause peak distortion (D) due to these edge effects, while the chosen geometry (3D Repeller, C) performs similarly to the 2D models. Lastly, the ATD simulated in the chosen geometry (C) is compared with the experimental data obtained from the real device (E). The performance of the real system is in reasonably good agreement with the result from the 3D Repeller model. The difference is primarily attributed to mechanical and electrical imperfections in the constructed device as well as minor IM peak distortions occurring on transit from the cIM device to the ToF analyser. In all the SIMION simulations, the ion-gas collisions were approximated by the SDS approach (Appelhans and Dahl, International Journal of Mass Spectrometry, 244 (2005) 1-14). Simulations A-D used a TW height of 35 V and a TW velocity of 375 m/s and a buffer gas pressure of 1.8 mbar (N_2). In all the simulations, arrival times of 20,000 ions were histogrammed with 60 µs bin width. Experimental data (E) were acquired at pressure of 2 mbar N_2, TW height of 35V and TW velocity of 375 m/s. In order to calculate the R(CCS/ΔCCS) values, a normal distribution peak function was fitted to each ATD. Using the difference between their centroids, a CCS/ms conversion factor was calculated and the measured peak FWHM was converted to CCS units (ΔCCS). R(CCS/ΔCCS) values for both peaks were then calculated and the average of the two values reported.

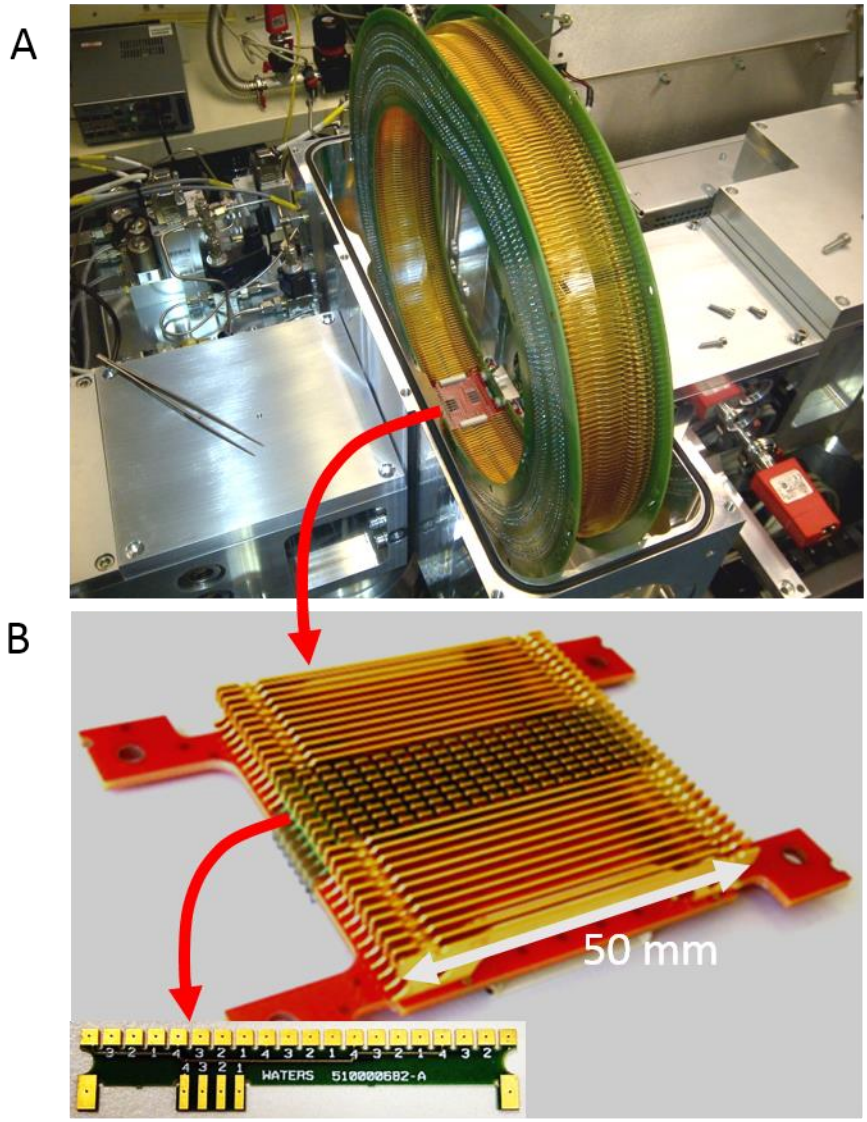

Figure S5. Instrument photographs. (A) the cIM device. (B) The multi-function array. The segmented array electrodes are made from edge plated PCBs (inset). These are soldered to the PCB substrate (red) which also consist of electrodes resembling those in the main cIM.

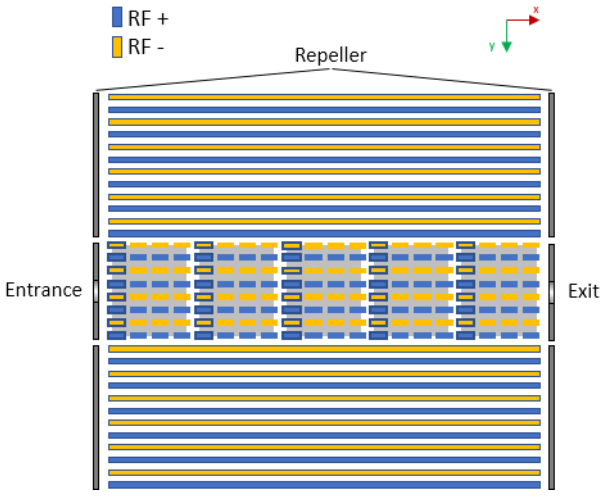

Figure S6. Schematics of layout and voltages applied in the array region. 180° RF phases applied to electrodes (yellow and blue). Array electrodes: repeat pattern of five sections (grey boxes).

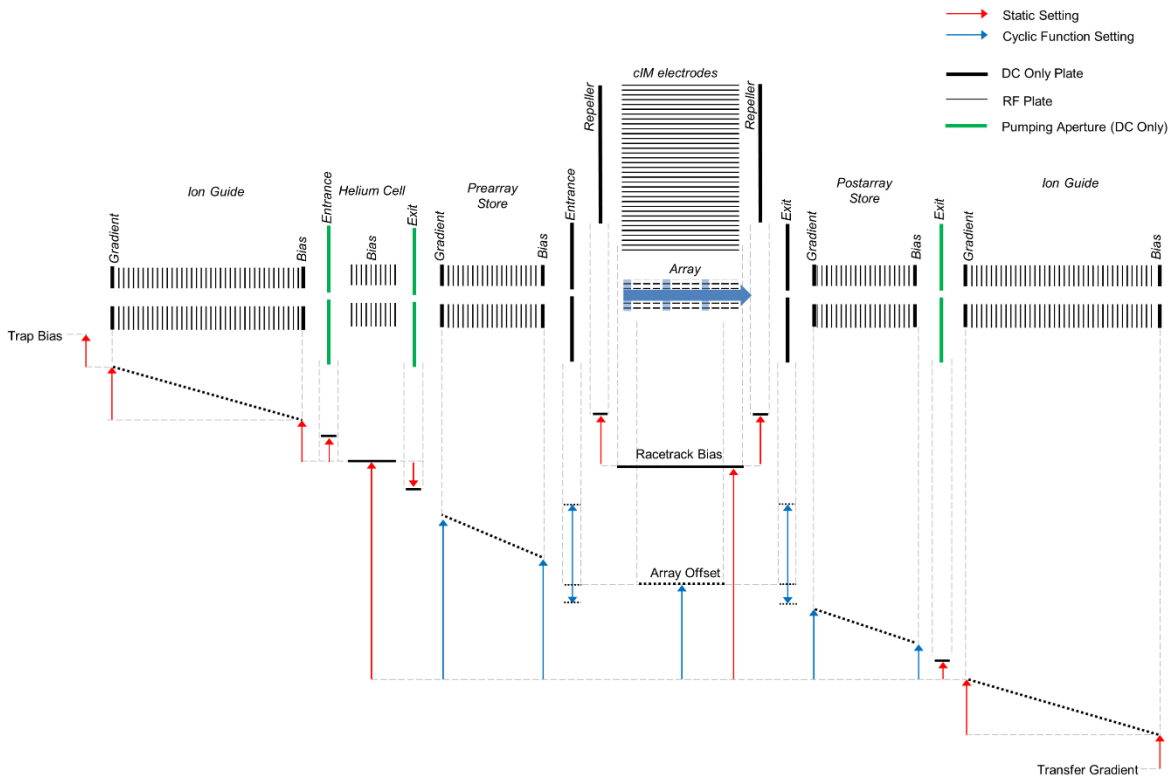

Figure S7. Potential energy (PE) diagram showing the voltages applied between the trap and transfer ion guides on the cIM instrument. Those settings which can be changed on a “per function” basis are indicated by blue arrows. Settings changeable on a “per sequence” basis are indicated by red arrows. The array entrance and exit aperture electrodes are shown schematically as physically offset to the repeller electrodes. This is only to allow representation of the corresponding voltage levels on this 2D schematic, in practice they are physically in-line, forming part of the repeller band during IM separation (see Figure S6).

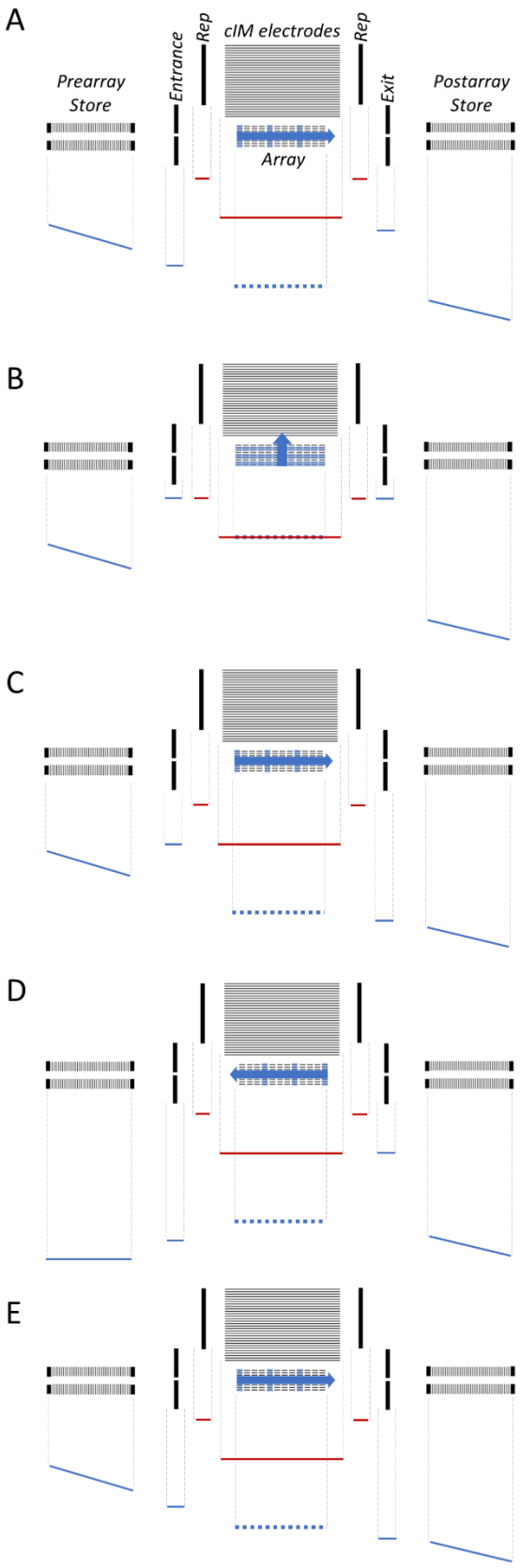

Figure S8. Potential energy schematics of the cIM functions. A: Injection. B: Separation. C: Ejection to ToF. D: Ejection to prearray store. E: Bypass. Settings changeable on a "per function" basis: blue lines. Settings changeable on "per sequence" basis: red lines. Blue arrows indicate the array TW direction.

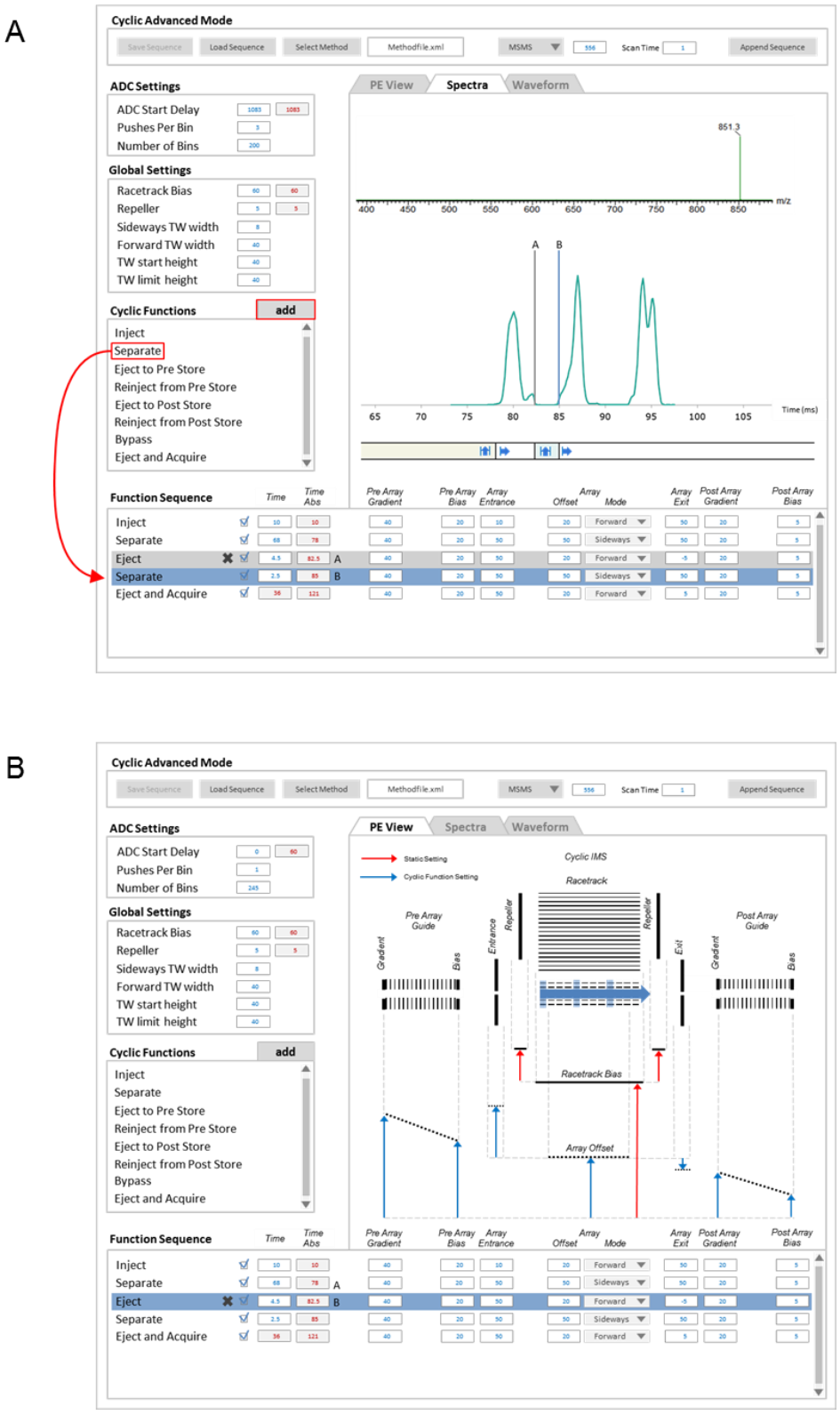

Figure S9. The cIM graphical user interface (GUI). Novel experiments can be set up by selecting functions from a pre-defined list and adding them into a function sequence (A, red arrow). In the "Spectra" view (A) the function sequence is represented by a bar chart overlaid with the "real time" arrival time distribution (ATD) display, enabling adjustment to the duration of each function as required. For example, the user can adjust function durations to "IM isolate" the required subset of the ATD (shown above) or perform an IMS^n experiment. Once added into the sequence, function settings can be customised further. An interactive potential energy (PE) diagram is generated for each function (B). The sequence settings are arranged in a table, where columns are aligned with the arrows in the PE diagram, simplifying interaction and control of the instrument.

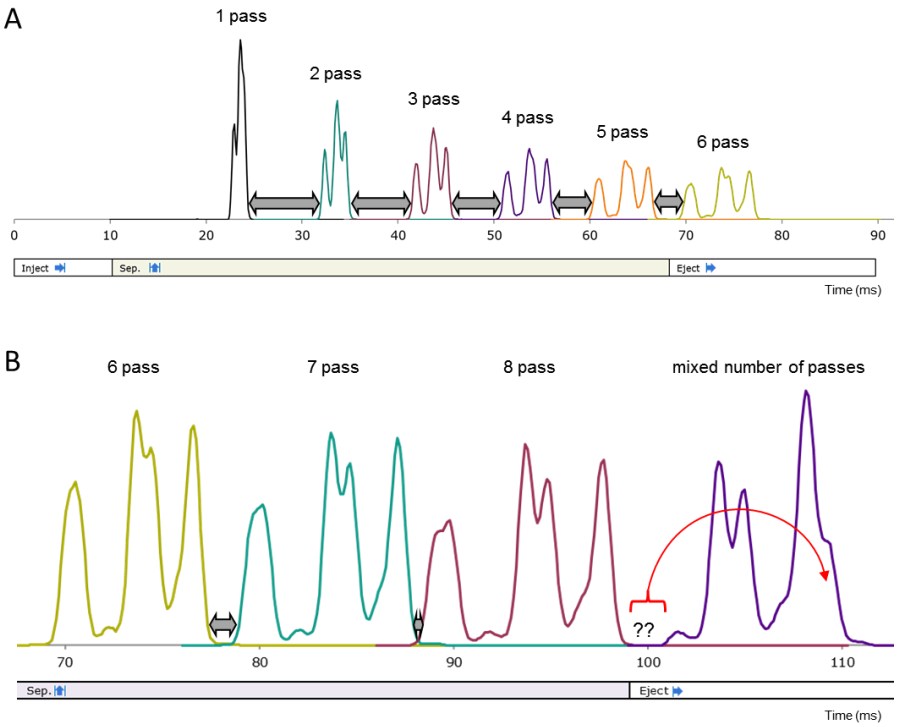

Figure S10. "Wrap around" effect in the cyclic IMS. (A) ATDs of the three pentasaccharides after 1-6 passes around the cIM. Resolution increases with increasing number of passes and new components are resolved. Importantly, the temporal separation between adjacent ATDs decreases with increasing number of passes (grey arrows). Thus, the spatial separation between the leading and trailing edges of the ion clouds in the cIM is also decreasing. If the experiment time is increased further, such that ions undergo more than 8 passes (B), the fastest component wraps around and merges with the slowest component (indicated by the red arrow). This results in an ATD corresponding to a mixed number of passes. Here, the fastest component has completed 9 passes while remaining ions have completed 8 passes around the cIM. In general, "wrap around" is undesirable and operational steps can be taken to avoid this.

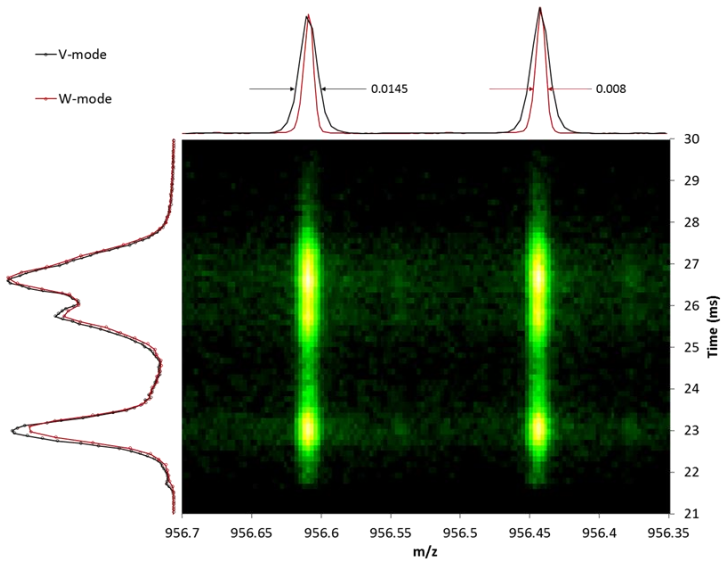

Figure S11. ToF resolution performance. A 2D IM-ToF spectrum of bovine insulin (6+) after 1 pass around the cIM measured in V-mode (black traces, R ~60,000) and W-mode (red traces, R ~100,000).

A

$$rCCS = \frac{\sqrt{\mu}\ CCS}{z}$$

Calibrants

m/z	Formula	Name	Arrival Time (ms)	$^{DT}CCS_{N2}$ (Å²)	rCCS (-)
455.29	$C_{27}H_{38}N_2O_4H$	Verapamil	10.56	208.8	1072.38
472.32	$C_{32}H_{41}NO_2H$	Terfenadine	12.65	228.7	1175.82
516.28	$C_{21}H_{37}N_7O_8H$	Polyalanine	10.48	211.0	1087.41
587.31	$C_{24}H_{42}N_8O_9H$	Polyalanine	12.42	228.0	1178.69
609.28	$C_{33}H_{40}N_2O_9H$	Reserpine	15.37	252.3	1305.39
658.35	$C_{27}H_{47}N_9O_{10}H$	Polyalanine	14.18	243.0	1259.33
729.39	$C_{30}H_{52}N_{10}O_{11}H$	Polyalanine	15.77	256.0	1329.35
800.43	$C_{33}H_{57}N_{11}O_{12}H$	Polyalanine	17.56	271.0	1409.56
871.46	$C_{36}H_{62}N_{12}O_{13}H$	Polyalanine	19.44	282.0	1468.79
942.50	$C_{39}H_{67}N_{13}O_{14}H$	Polyalanine	21.32	294.0	1533.10
1013.54	$C_{42}H_{72}N_{14}O_{15}H$	Polyalanine	23.12	306.0	1597.29
1084.57	$C_{45}H_{77}N_{15}O_{16}H$	Polyalanine	25.12	321.5	1679.67
1155.61	$C_{48}H_{82}N_{16}O_{17}H$	Polyalanine	27.05	333.6	1744.24

B

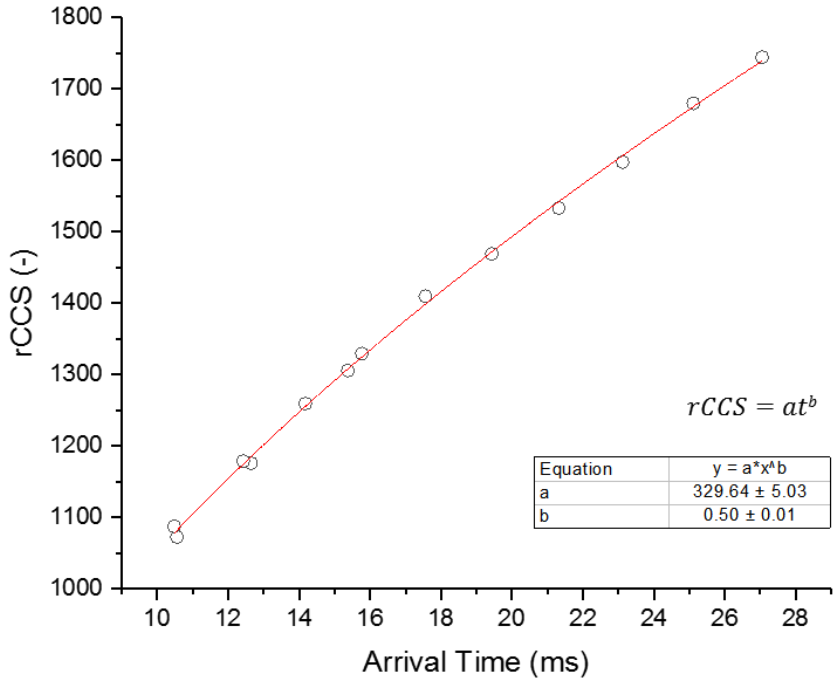

C

Test Analyte

m/z	Formula	Name	Arrival Time (ms)	$^{DT}CCS_{N2}$ (Å²)	$^{TW}CCS_{N2}$ (Å²)
556.28	$C_{28}H_{37}N_5O_7H$	Leu-Enkephalin	12.79	**229.3**	**230.9**

Figure S12. Collision Cross Section (CCS) calibration example. (A) Reduced CCS (rCCS) values have been computed for a range of calibrants (small molecule and polyalanine cations) using $^{DT}CCS_{N2}$ values measured with a Synapt G2Si instrument fitted with linear field IM drift cell. (B) Arrival times of the calibrants were then recorded after 1 pass around the cIM device (1.8 mbar of N_2, TW height of 35V and TW velocity of 375 m/s), plotted against rCCS and power law function was fitted to the data. (C) The arrival time of a test analyte (Leu-Enkephalin) was then measured under the same conditions and converted to a $^{TW}CCS_{N2}$ value using the fitted coefficients. The experimentally determined $^{TW}CCS_{N2}$ is in good agreement with the available value measured using the linear field IM drift cell (0.7% difference).

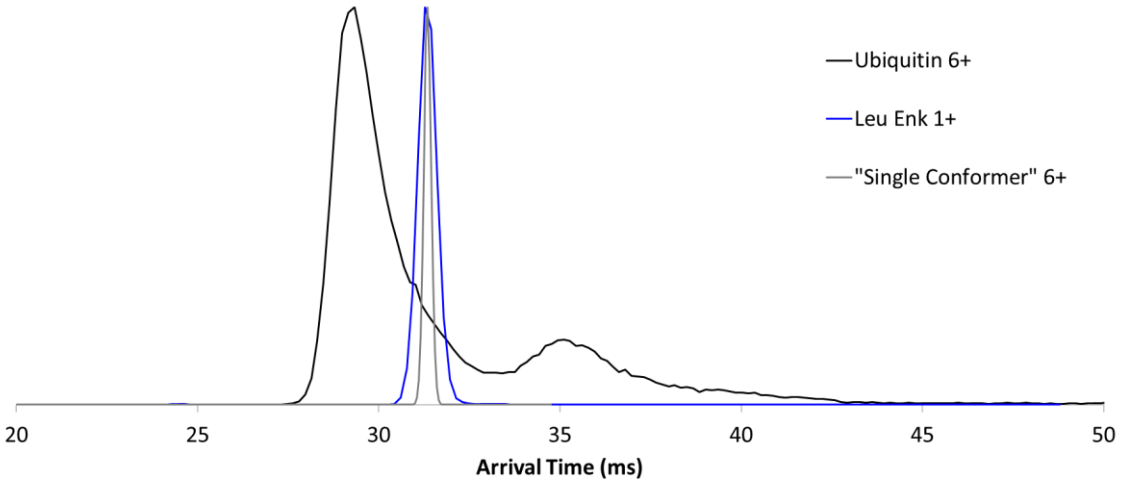

Figure S13. ATDs of the 6+ charge state of ubiquitin and the singly charged leucine enkephalin acquired with one pass around the cIM. As can be seen the width of the ubiquitin peak is significantly larger than that of the leucine enkephalin, indicating the presence of multiple conformations. For comparison, the calculated ATD of a 6+ species with a single conformation is shown. This estimate is based on the fact that the peak width of the 6+ charge state is expected to be narrower by a factor of √6. Arrival times were then recorded after 1 pass around the cIM device (2 mbar of N_2, TW height of 30V and TW velocity of 375 m/s).